ResearchGate

See discussions, stats, and author profiles for this publication at: https://www.researchgate.net/publication/283305887

Photoelectron Imaging Spectroscopy of AuC3H− Anions: Four Isomers

ARTICLE *in* THE JOURNAL OF PHYSICAL CHEMISTRY A · OCTOBER 2015

Impact Factor: 2.69 · DOI: 10.1021/acs.jpca.5b05122

READS

16

3 AUTHORS, INCLUDING:

Jing-Heng Meng

Chinese Academy of Sciences

14 PUBLICATIONS **56** CITATIONS

SEE PROFILE

Sheng-Gui He

Chinese Academy of Sciences

153 PUBLICATIONS **2,491** CITATIONS

SEE PROFILE

Available from: Jing-Heng Meng

Retrieved on: 26 January 2016

THE JOURNAL OF PHYSICAL CHEMISTRY A

Article

pubs.acs.org/JPCA

Photoelectron Imaging Spectroscopy of AuC_3H^- Anions: Four Isomers

Jing-Heng Meng,[†,‡] Qing-Yu Liu,[†,‡] and Sheng-Gui He*[,†]

[†]Beijing National Laboratory for Molecular Sciences, State Key Laboratory for Structural Chemistry of Unstable and Stable Species, Institute of Chemistry, Chinese Academy of Sciences, Beijing 100190, People's Republic of China

[‡]University of Chinese Academy of Sciences, Beijing 100049, People's Republic of China

Supporting Information

ABSTRACT: Laser ablation generated AuC_3H^- anions were skimmed into a time-of-flight mass spectrometer (TOF-MS) and selected with a mass gate. Photoelectron spectra of AuC_3H^- were recorded using the velocity map imaging technique at several photon energies. The experimental spectra, quantum chemistry calculations, and Franck–Condon simulations suggest that the AuC_3H^- cluster has four structure isomers, including one unexpected structure of $[C{=}C{=}C{-}Au{-}H]^-$. When AuC_3H^- is compared with $C_3H_2^-$, introduction of gold into the hydrocarbon system results in the much lower isomerization barriers.

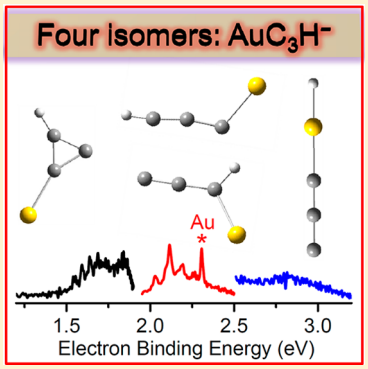

1. INTRODUCTION

The chemistry of gold has been rapidly developed since the discovery of high activity and selectivity of nanostructured gold[1−4] and the strong relativistic effects of gold.[5] As an important research branch of gold, homogeneous gold catalysis has been increasingly investigated in organic synthesis and a lot of review articles can be found.[6−11] Fundamental study of the gold−carbon bonding is of great significance to understand the catalytic mechanisms. With the aid of photoelectron spectroscopy (PES)[12,13] and theoretical calculations, well-defined organogold clusters can serve as model systems to probe the nature of the bonding between gold and carbon.

So far, many theoretical studies on Au−C clusters, including Au_nC^- (n = 1−10),[14] AuC_n (n = 1−11),[15] AuC,[16] $C_2Au_n^+$ (n = 1, 3, 5),[17] C_2Au_n (n = 2, 4, 6),[17] C_nAu_m (n,m = 1,4; 2,2; 2,4; 2,6; 6,6),[18] CAu_{16}^q (q = −1, 0),[19] CAu_4,[20] C_5Au_{12},[21] CAu_2^{2+},[22] CAu_3^+,[22] and AuC^+[23] have been carried out. Note that all of these investigations mainly focus on the geometric and electronic structures. Among these contributions, Sun et al. studied the dissociation channels for AuC_n (n = 1−11) clusters as well.[15] Pal et al. identified Au/H analogy in CAu_4 cluster.[20] Later, Li et al. extended Au/H analogy to Au_3/H anology in $C_2Au_n^+$ (n = 1, 3, 5) and C_2Au_n (n = 2, 4, 6).[17] On the other hand, very few experimental investigations on Au−C clusters[24−28] have been performed. The generation of $Au_nC_m^{\pm}$ clusters is the topic for most of the contributions,[24−27] and the photodissociation of $Au_nC_m^+$ at 355 nm was carried out by Duncan and co-workers.[28] To the best of our knowledge, the experimental spectroscopic study on Au−C clusters has been scarcely reported. Only $LAuCCH^-$ (L = Cl, I, CCH)[29] and AuC_2^-[30,31] have been recently studied by the PES method. Herein, to further understand the bonding between gold and carbon substrate we present an investigation on AuC_3H^- anion, which may be considered as the single-Au analogue of C_3H_2 carbene.[32] The PE imaging spectroscopy in conjunction with density functional theory (DFT) calculations was employed and the details are given below.

2. METHODS

2.1. Experimental Methods. The $Au_xC_yH_z^-$ cluster ions were generated by laser ablation of a rotating and translating gold metal disk in the presence of about 0.5% CH_4 seeded in a helium (99.99% purity) carrier gas with a backing pressure of 7 atm. A 532 nm (second harmonic of Nd^{3+}:YAG) laser with an energy of 5−8 mJ/pulse and a repetition rate of 10 Hz was used. The carrier gas was controlled by a pulsed valve (General Valve, Series 9). After multiple collisions with the carrier gas in the narrow cluster formation channel and supersonic expansion, the rotational temperature of the cluster can be much lower than the room temperature while the vibrational temperature can be high. Our previous experiments indicated that the cluster vibrational temperature is around 300 K.[33] The generated cluster ions were skimmed into a time-of-flight mass spectrometer (TOF-MS).[34,35] Next, the cluster ions passed through two identical reflectors with a Z-shaped configuration in the primary TOF-MS and then the ions of interest (AuC_3H^-) were selected with a mass gate to interact

Received: May 29, 2015
Revised: October 27, 2015

ACS Publications © XXXX American Chemical Society

DOI: 10.1021/acs.jpca.5b05122
J. Phys. Chem. A XXXX, XXX, XXX−XXX

with a wavelength-tunable laser beam delivered from an OPO (optical parametric oscillator, Continuum, Horizon) laser source. The OPO laser wavelengths were determined using a grating spectrograph (Acton SpectraPro 500I) calibrated with the atomic spectral lines of a mercury−argon lamp.[36] The photoelectron spectrometer was calibrated with the known spectrum of Au^-.[37] The energy resolution is 3.0% at kinetic energy E_k = 1.0 eV. The details of the PE imaging spectrometer can be found in ref 35.

2.2. Computational Methods. The DFT calculations with Gaussian 09 program[38] were performed. The TZVP basis sets[39] were employed for C and H atoms. For Au atom, a D95V basis set[40] combined with the Stuttgart/Dresden relativistic effective core potential (denoted as SDD in Gaussian software) was used. The TPSS functional[41] was used in this study as in other contributions[42−44] involving Au, C, and H elements. For the gold-containing polyatomic systems, the spin−orbit effect may be neglected for Au. For example, the vertical detachment energies (VDEs) of $LAuCCH^-$ (L = Cl, I, CCH)[29] are overestimated by less than 6.5% without spin−orbit corrections. The coupled-cluster method with single, double, and perturbative triple excitations [CCSD(T)][45,46] was also used to calculate the single-point energies of selected cluster structures optimized by the DFT. The transition states (TSs) were optimized by using the Berny algorithm method.[47] Intrinsic reaction coordinate calculations[48,49] were also performed so that each TS connects two appropriate local minima. Vibrational frequency calculations were carried out to check that reaction intermediates and TSs have zero and only one imaginary frequency, respectively. The zero-point vibration corrected energies (ΔH_0) were reported in this study. The DFT calculated geometrical and vibrational data were used in the Franck−Condon (FC) simulations of the PE spectra. The FC simulations were performed with the ezSpectrum software suite[50] using the Dushinsky approximation. The vibrational excited states of both anionic and neutral AuC_3H were considered with FC simulations. The convolution resolution of 20 meV and the temperature of 300 K were applied to obtain the simulated spectra. The time-dependent DFT (TD/DFT) method was also used to predict the vertical excitation energies from the anion ground state to the neutral electronic excited states.

3. RESULTS

3.1. Experimental Results. Figure 1A shows a typical TOF mass spectrum for the distribution of the $Au_xC_yH_z^-$ anions generated by laser ablation cluster source. Species of Au^-, AuC_2^-, AuC_3H^-, and AuC_4^- et al. can be assigned. With a mass gate, the AuC_3H^- anion of interest was mass-selected as shown in Figure 1B. Figure 2 shows original velocity map images (left panels) and the corresponding PE spectra (right panels) of AuC_3H^- at laser wavelengths of 650 nm (1.91 eV), 480 nm (2.58 eV), and 385 nm (3.22 eV). For the spectrum in Figure 2A recorded at 650 nm, four identified spectral features that are separated by a constant energy spacing of about 371 cm^{-1} are assigned to a single vibrational progression in the upper state (i.e., neutral AuC_3H). Note that the binding energy of the first peak labeled "a" is 1.549 eV. The significant signals near threshold labeled with asterisk can be due to another electronic transition. For the spectrum in Figure 2B collected at 480 nm, the peak positions and pattern match that in Figure 2A in the binding energy range of 1.4 to 1.9 eV, albeit at a reduced resolution that is due to the higher photoelectron kinetic

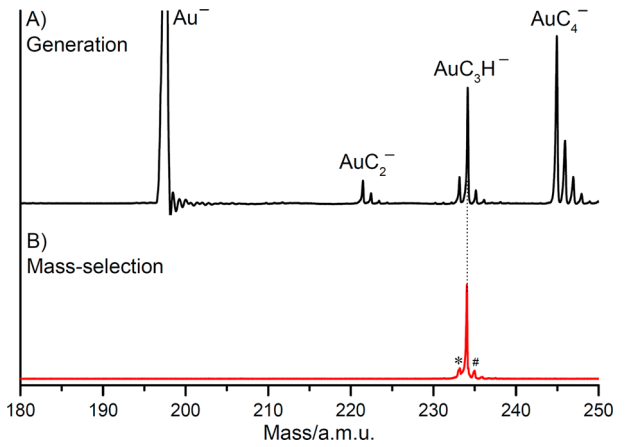

Figure 1. TOF mass spectra for the generation of $Au_xC_yH_z^-$ anions (A) and the mass-selection of AuC_3H^- (B). The signals labeled with "*" and "#" in panel B represent the residual impurity of AuC_3^- ion and the contribution of $Au^{13}C^{12}C_2H^-$ isotopomer, respectively.

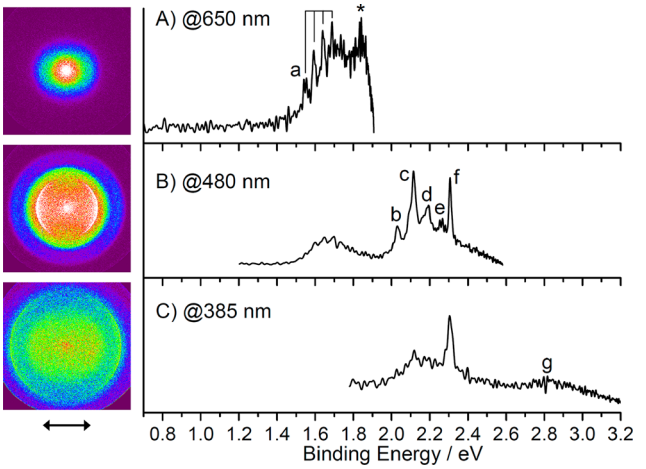

Figure 2. Photoelectron images and spectra of AuC_3H^- at laser wavelengths of 650 nm (A), 480 nm (B), and 385 nm (C). The left panels show the raw photoelectron images. The double arrow indicates the polarization of the laser.

energies. In the binding energy range of 1.9 to 2.6 eV, five spectral features labeled "b−f" are identified. It is worthy to note that the "f" peak with binding energy of 2.307 eV is very sharp with respect to the "b−e" peaks. The sharp "f" peak is assigned as the $^2S_{1/2} \leftarrow {}^1S_0$ transition of Au^- anion, which derives from the photodissociation of AuC_3H^- ($AuC_3H^- + h\nu \rightarrow Au^- + C_3H$). This result will be discussed in detail later. The binding energies of these observed peaks are summarized in Table 1. The energy spacing between the "b−e" peaks is different, suggesting that they do not derive from a single vibrational progression. For the spectrum recorded at 385 nm shown in Figure 2C, a new broad spectral feature labeled "g" with the central binding energy of 2.808 eV can be identified, even though the signal-to-noise ratio of this peak is low.

In addition to the high-resolution capability, another important advantage of PE imaging is that it can give the angular distribution of the photoelectrons.[12] For one-photon detachment, the degree of anisotropy is characterized by the angular dependent intensity, $I(\theta)$, defined by

$$dI(\theta) \sim [1 + \beta P_2(\cos\theta)] \quad (1)$$

DOI: 10.1021/acs.jpca.5b05122
J. Phys. Chem. A XXXX, XXX, XXX−XXX

Table 1. Observed Binding Energies from the PE Spectra of AuC_3H^- (Figure 2)[a]

observed peaks	binding Energies (eV)	β
a	1.549	> 0
b	2.031	> 0
c	2.115	
d	2.187	
e	2.260	> 0
f	2.307	> 0 (1.7)
g	2.808	> 0

[a]The signs for the anisotropy parameter (β) are indicated.

where $P_2(\cos\theta) = (3\cos^2\theta - 1)/2$ is the second order Legendre polynomial, θ is the angle between the direction of the laser polarization and that of the ejected electron, and β is the anisotropy parameter. The β parameter denotes the degree of alignment between the direction of the polarization of the detachment laser and the photodetached electrons. The β values observed from the PE images in left panels of Figure 1 for the "a−g"peaks are all positive (>0), except for the "c" and "d" peaks of which the β values are difficult to determine. It is worthy to note that the β parameter of the "f" peak is as large as 1.7 (Table 1).

Because the AuC_3^- ion is present after mass selection (Figure 1B, labeled with an asterisk), the PES spectra of AuC_3^- have also been recorded at 480 and 385 nm (see Figure S1 in the Supporting Information). It turns out that AuC_3^- can contribute a little intensity to the "f" and "g" peaks in Figure 2.

3.2. Computational Results. Several types of geometric structures for AuC_3H^- were calculated by the DFT and the eight most stable structures denoted as I0n (n = 1−8) are given in Figure 3. The doublet states (M2) are found to be more stable than the corresponding quartet states (M4) for all the structures. Surprisingly, a quasi-linear structure of C═C═C−Au−H (I01) has the lowest energy. To the best of our knowledge, the bonding of gold in I01 is rather unusual and this structure may be interesting for further theoretical study. We have analyzed the molecular orbitals of I01 as well and the results are shown in Figure S3 (Supporting Information). The following three isomers (I02−I04) can also be populated in the cluster source because their energies are within 0.4 eV relative to that of I01. The isomers of I05−I08 are not discussed below because they have higher relative energies (more than 1.3 eV).

The relative energies of I01−I08 isomers by the CCSD(T) single point calculations are generally consistent with the results of the DFT calculations. The I04 structure becomes the most stable among I01−I04, suggesting that I04 is the lowest-lying isomer of AuC_3H^-.

The initial and final electronic states along with the adiabatic detachment energies (ADEs) and VDEs for the I01−I04 isomers are given in Table 2. Doublet state is assigned for the initial state, while singlet and triplet final states were all calculated. For I01, $^2A'$ state is the initial ground state and $^1A'$ state is considered as the final ground state. The $^3A''$ state is not discussed further because of its higher relative energy with respect to $^1A'$ state. Similarly, for I02 and I04, the singlet states are assigned for the final ground states. On the basis of the DFT calculated results, the ^3A state of I03 (AuCCCH) is slightly more stable than the ^1A state (by 0.24 eV), which is in agreement with the fact that the HCCCH molecule has a triplet ground state.[51] Both the singlet and triplet electronic states of the I03 isomer may be reached in our experiments. The geometric patterns and relative energies for neutral I02−I04 (AuC_3H) are similar to those of the C_3H_2 carbene,[32] resulting a gold/hydrogen analogy.

Table 2. Electronic States and Photodetachment Energies (in unit of eV) for I01−I04 Isomers of AuC_3H^- (Figure 3)

isomer	initial state	final state	ADE (eV)	VDE (eV)
I01	$^2A'$	$^1A'$	2.822	2.863
		$^3A''$	5.885	6.335
I02	^2A	^1A	2.096	2.244
		^3A	3.219	3.364
I03	^2A	^1A	2.015	2.307
		^3A	1.776	2.094
I04	$^2A'$	$^1A'$	1.372	1.480
		^3A	2.839	3.351

The FC simulations are widely performed to identify the geometric and electronic structures of clusters. Figure 4 shows the comparison of the FC simulated spectra for I01−I04 isomers with the experimental spectra. As shown in Figure 4A, for the $^1A' \leftarrow {}^2A'$ transition of I04, the Au−C stretching mode of neutral molecule with frequency of 367.5 cm^{-1} dominates the simulated spectrum, which is well consistent with the experimentally observed spacing of 371 cm^{-1} recorded at 650

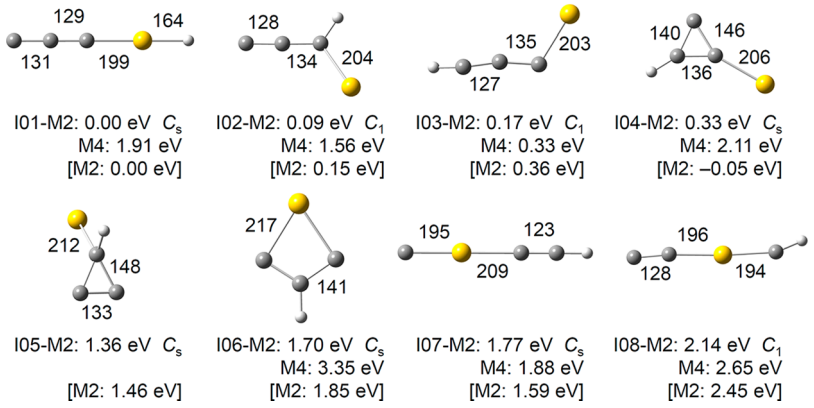

Figure 3. DFT calculated isomers of AuC_3H^- at doublet and quartet states. The zero-point vibration corrected energies (eV) with respect to the most stable isomer (I01-M2) are given. The point groups and bond lengths (in pm) are shown. Relative energies by CCSD(T) single point calculations with DFT-optimized geometries are given in square brackets.

DOI: 10.1021/acs.jpca.5b05122
J. Phys. Chem. A XXXX, XXX, XXX−XXX

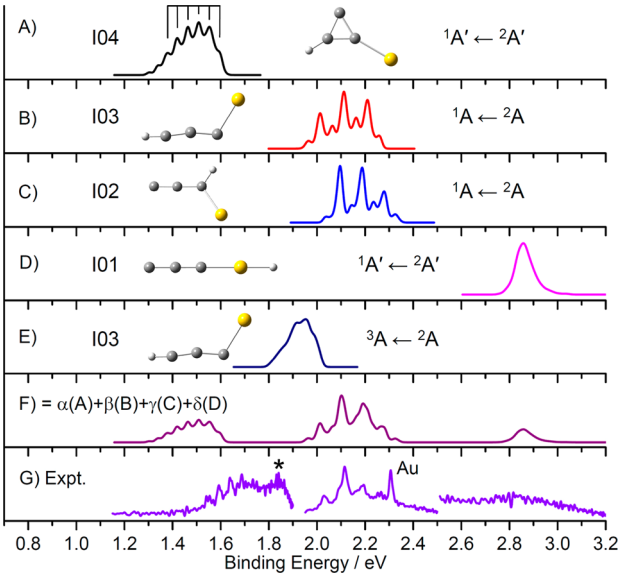

Figure 4. Franck−Condon simulations of the PE spectra. The transitions for I01−I04 isomers are shown in panels (A−E). Panel (F) gives the simulated spectra. Panel (G) shows the experimental spectra composed of the spectra in Figure 2A−C. The intensities of the three bands have been scaled.

nm (Left spectrum in Figure 4G) with an ADE shift by about 0.18 eV. For the ^{1}A ← ^{2}A transition of I03 and I02 (Figure 4B,C), the C−H bending modes of neutral molecules dominate the simulated spectra with frequencies of 793.6 and 748.7 cm^{-1}, respectively. However, neither of the FC spectra shown in Figure 4B,C can interpret the experimental spectrum collected at 480 nm (center spectrum in Figure 4G) because of the relatively large difference in the energy spacing. When these two FC spectra combine together by a suitable ratio (5:2) as shown in Figure 4F, the FC spectrum from 1.9 to 2.4 eV fits well with the experimental spectrum (center spectrum in Figure 4G). The FC simulated spectrum for the ^{1}A′ ← ^{2}A′ transition of I01 is shown in Figure 4D. It can be seen that this is a broad peak with binding energy centered at 2.856 eV, which is in agreement with the experimental spectrum recorded at 385 nm (right spectrum in Figure 4G). Note that the Cartesian coordinates of the DFT calculated I01−I04 isomers in anionic (doublet) and neutral (singlet) states are given in Table S1 (Supporting Information). As mentioned above, the triplet state of neutral I03 may also be reached in the experiment, so the FC simulations for the ^{3}A ← ^{2}A transition of I03 were also performed and the result is shown in Figure 4E. The spectral feature labeled with the asterisk in Figures 2A and 4G can be due to this transition, while it becomes relatively weak in Figure 2B. The vertical transitions from the ground state of anion to different electronic excited states of the neutral have been calculated by the TD/DFT method and the results are given in Table S2 (Supporting Information). For I01, I02, and I04, the energies of the electronic excited states of neutral with respect to that of the corresponding ground state of anion are larger than 3.18 eV, and the transitions from the ground state of anion to electronic excited states of neutral were not observed by our PES experiment. For I03, the vertical transition energy from the ground state (^{2}A) of anion to the first electronic excited state (^{1}A) of neutral is 2.884 eV thus this transition may have some contribution to the "g" peak in Figure 2C. Nevertheless, the observed experimental PE spectra can be generally interpreted on the basis of the transitions of the four cluster isomers.

4. DISCUSSION

4.1. Gold Anion Generation by Photodissociation. In Figure 2B, the sharp "f" peak with binding energy of 2.307 eV is assigned as $^2S_{1/2} \leftarrow {}^1S_0$ transition of the Au^- anion, which can be the photodissociation product of AuC_3H^-. The calculated bond dissociation energies for I02−I04 isomers of AuC_3H^- are given in Table 3. Two dissociation channels, namely, C_3H^- + Au and C_3H + Au^-, were calculated. It can be seen that the C_3H + Au^- dissociation channel is more favorable by more than 0.3 eV than the other channel for all the three isomers. Then, the Au^- anion was photodetached by another photon and the photoelectron from the photodetachment of Au^- was detected by our PE imaging spectrometer. This hypothesis is confirmed by our experimental observations. The photodissociation mass spectrum of the mass-selected AuC_3H^- ion has been recorded at 480 nm and the results are given in Figure S2 (Supporting Information). The Au^- + C_3H channel is the only photodissociation channel for the AuC_3H^- ion (Supporting Information Figure S2c). Additionally, the Au^- + C_3 channel is the only photodissociation channel for the AuC_3^- ion (Supporting Information Figure S2b). It is worthy to point out that the photon energy of 480 nm is 2.583 eV, which is larger than the bond dissociation energy of (Au^-−C_3H) and the well-determined electron affinity (EA) of Au atom (2.309 eV).[37] This is very consistent with our experimental results that the β parameter of "f" peak is positive (1.7) and the binding energy of "f" peak (2.307 eV) is less than the well-determined EA of Au atom by only 2 meV, which is within the precision of our apparatus (±5 meV).[35] The Au^- anion generation from I01 ($CCCAuH^-$) by photodissociation is difficult and the C_3^- + AuH channel for I01 has a dissociation energy of 2.889 eV on the basis of the DFT calculations.

Table 3. Bond Dissociation Energies for I02−I04 Isomers of AuC_3H^- (Figure 3)

isomer	C_3H^- + Au (eV)	C_3H + Au^- (eV/nm)
I02	2.609	2.255/549.8
I03	2.532	2.187/566.9
I04[a]	2.434	1.961/632.2

[a]The C_3 unit in $[C_3H]^{-/0}$ is cyclic.

4.2. Isomerization of AuC_3H^- Isomers. In homogeneous catalysis, introduction of gold into organic substrate can result in much easier chemical transformations. Isomerizations among I01−I04 structures of AuC_3H^- are shown in Figure 5A. The energy barriers for I01 → I02, I02 → I03, and I03 → I04 transformations are 2.22 eV (TS1), 1.71 eV (TS2), and 1.96 eV (TS3), respectively. For a comparison, the isomerization of $C_3H_2^-$ anion has also been calculated under the TPSS/TZVP level. Four isomers, labeled as IS1, IS2, IS2′, and IS3, at the doublet state are shown in Figure 5B. The IS1 has the lowest energy and the IS3 has the highest energy of 1.71 eV relative to the IS1. The IS2 and IS2′ have similar energies and geometric structures and can transform to each other very easily (IS2′ → TS5 → IS2), thus, only one of them will be discussed in the text below. The PES experiment reported the EAs of 1.796 eV[52] and 1.156 eV[32] for neutral IS1 and IS2, respectively, while there is no experimental work reporting the EA of neutral IS3 until now. This is due to the much higher energy of IS3 with

DOI: 10.1021/acs.jpca.5b05122
J. Phys. Chem. A XXXX, XXX, XXX−XXX

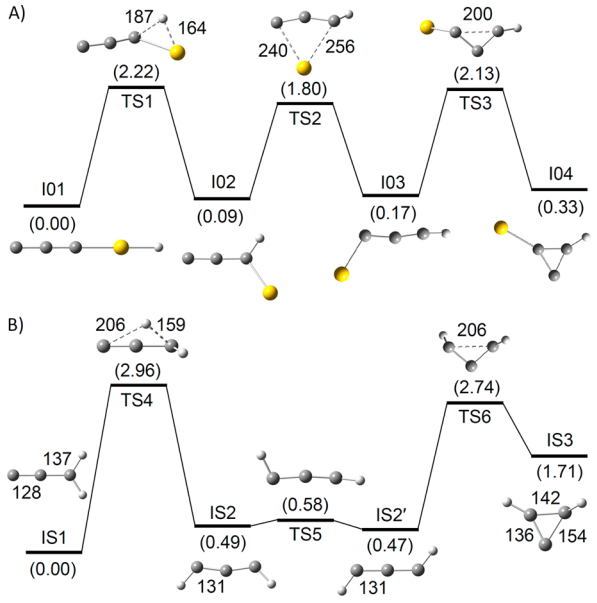

Figure 5. DFT calculated potential energy profiles of isomerizations at doublet state for AuC_3H^- (A) and $C_3H_2^-$ (B). The zero-point vibration corrected energies (eV) with respect to I01 in (A) and IS1 in (B) are given. Some bond lengths are shown in picometers.

respect to IS1 (1.71 eV, Figure 5B), leading to the difficult generation of the IS3 isomer. Note that the quartet states for IS1, IS2, and IS3 (IS1−IS3) have much higher energy than the doublet states by 3.318, 2.323, and 2.403 eV, respectively, based on the DFT calculations.

Isomerizations in ^{13}C-labeled neutral IS1−IS3 of C_3H_2 carbene have been studied by photolysis with the aid of IR spectroscopy.[53,54] The theoretical results (Figure 5B) indicate that the largest energy barriers of isomerization of $C_3H_2^-$ (IS1−IS3) is 2.96 eV (TS4), which is higher than the highest isomerization barriers of AuC_3H^- (I01−I04) by 0.74 eV (TS1, see Figure 5A). Therefore, introduction of gold into hydrocarbon molecules can result in much lower isomerization barriers. This may be one important nature of gold catalysis.[6−11]

5. CONCLUSIONS

The geometric and electronic structures of AuC_3H^- anions have been investigated using photoelectron imaging spectroscopy and density functional theory calculations. Four isomeric structures of AuC_3H^- have been identified. The Franck−Condon simulations identify that the $^1AuC_3H \leftarrow {}^2AuC_3H^-$ transitions dominate the observed experimental spectra. The free gold anion is generated by photodissociation of AuC_3H^- at 480 nm and lower wavelengths. When AuC_3H^- is compared with $C_3H_2^-$, an unexpected structure of $CCCAuH^-$ is proposed and the Au/H analogy is found for three other cluster isomers. Introduction of gold into hydrocarbon molecules can result in the much lower isomerization barriers.

■ ASSOCIATED CONTENT

Supporting Information

The Supporting Information is available free of charge on the ACS Publications website at DOI: 10.1021/acs.jpca.5b05122.

The PES spectra of AuC_3^- at laser wavelengths of 480 and 385 nm, the TOF mass spectra for photoreactions of the mass-selected AuC_3^- and AuC_3H^- ions at 480 nm, the molecular orbitals of I01, the Cartesian coordinates of the DFT calculated cluster isomers (I01−I04), the vertical excitation energies of five lowest-lying electronic excited states of the neutral with respect to that of the corresponding ground state of anion, and the complete author lists of references of 32, 38, and 52. (PDF)

■ AUTHOR INFORMATION

Corresponding Author

*E-mail: shengguihe@iccas.ac.cn. phone: +86-10-62568330. fax: +86-10-62559373.

Notes

The authors declare no competing financial interest.

■ ACKNOWLEDGMENTS

This work was supported by Chinese Academy of Sciences (Nos. YZ201318, XDA09030101), the National Natural Science Foundation of China (Nos. 21325314, 21203208), and Major Research Plan of China (Nos. 2013CB834603 and 2011CB932302).

■ REFERENCES

(1) Bond, G. C.; Sermon, P. A. Gold Catalysts for Olefin Hydrogenation. *Gold Bull.* **1973**, *6*, 102−105.
(2) Haruta, M.; Kobayashi, T.; Sano, H.; Yamada, N. Novel Gold Catalysts for the Oxidation of Carbon Monoxide at a Temperature Far below 0 °C. *Chem. Lett.* **1987**, *16*, 405−408.
(3) Hutchings, G. J. Vapor Phase Hydrochlorination of Acetylene: Correlation of Catalytic Activity of Supported Metal Chloride Catalysts. *J. Catal.* **1985**, *96*, 292−295.
(4) Ishida, T.; Haruta, M. Gold Catalysts: Towards Sustainable Chemistry. *Angew. Chem., Int. Ed.* **2007**, *46*, 7154−7156.
(5) Pyykkö, P. Theoretical Chemistry of Gold. III. *Chem. Soc. Rev.* **2008**, *37*, 1967−1997.
(6) Hashmi, A. S. K. Gold-Catalyzed Organic Reactions. *Chem. Rev.* **2007**, *107*, 3180−3211.
(7) Jiménez-Núñez, E.; Echavarren, A. M. Gold-Catalyzed Cycloisomerizations of Enynes: A Mechanistic Perspective. *Chem. Rev.* **2008**, *108*, 3326−3350.
(8) Gorin, D. J.; Sherry, B. D.; Toste, F. D. Ligand Effects in Homogeneous Au Catalysis. *Chem. Rev.* **2008**, *108*, 3351−3378.
(9) Arcadi, A. Alternative Synthetic Methods through New Developments in Catalysis by Gold. *Chem. Rev.* **2008**, *108*, 3266−3325.
(10) Li, Z.; Brouwer, C.; He, C. Gold-Catalyzed Organic Transformations. *Chem. Rev.* **2008**, *108*, 3239−3265.
(11) Corma, A.; Leyva-Pérez, A.; Sabater, M. J. Gold-Catalyzed Carbon−Heteroatom Bond-Forming Reactions. *Chem. Rev.* **2011**, *111*, 1657−1712.
(12) León, I.; Yang, Z.; Liu, H.-T.; Wang, L.-S. The Design and Construction of a High-Resolution Velocity-Map Imaging Apparatus for Photoelectron Spectroscopy Studies of Size-Selected Clusters. *Rev. Sci. Instrum.* **2014**, *85*, 083106.
(13) Neumark, D. M. Slow Electron Velocity-Map Imaging of Negative Ions: Applications to Spectroscopy and Dynamics. *J. Phys. Chem. A* **2008**, *112*, 13287−13301.
(14) Yan, L.-L.; Liu, Y.-R.; Huang, T.; Jiang, S.; Wen, H.; Gai, Y.-B.; Zhang, W.-J.; Huang, W. Structure, Stability, and Electronic Property of Carbon-Doped Gold Clusters Au_nC^- (n = 1−10): A density Functional Theory Study. *J. Chem. Phys.* **2013**, *139*, 244312.
(15) Sun, X.; Du, J.; Jiang, G. Au-Doped Carbon Clusters AuC_n with n = 1−11: A Theoretical Investigation. *Struct. Chem.* **2013**, *24*, 1289−1295.
(16) Li, Z.; Zhang, J.; Meng, D.; Yu, Y. Electronic Structure and Bonding Characters of the Two Lowest States of Copper, Silver, and Gold Monocarbides. *Comput. Theor. Chem.* **2011**, *966*, 97−104.

DOI: 10.1021/acs.jpca.5b05122
J. Phys. Chem. A XXXX, XXX, XXX−XXX

(17) Li, D.-Z.; Li, S.-D. A Density Functional Investigation on $C_2Au_n^+$ (n = 1, 3, 5) and C_2Au_n (n = 2, 4, 6): from Gold Terminals, Gold Bridges, to Gold Triangles. *J. Cluster Sci.* **2011**, *22*, 331−341.
(18) Zaleski-Ejgierd, P.; Pyykkö, P. Bonding Analysis for Sterically Uncongested Simple Aurocarbons C_nAu_m. *Can. J. Chem.* **2009**, *87*, 798−801.
(19) Fa, W.; Yang, A. Detecting the Lowest-Energy Structures of CAu_{16}^q (q = − 1, 0). *Phys. Lett. A* **2008**, *372*, 6392−6395.
(20) Pal, R.; Bulusu, S.; Zeng, X.-C. Exploring the Lowest-Energy Structures of Group IV Tetra-Aurides: XAu_4 (X = C, Si, Ge, Sn). *J. Comput. Methods Sci. Eng.* **2007**, *7*, 185−193.
(21) Naumkin, F. Nano-Jewellery: C_5Au_{12}−A Gold-Plated Diamond at Molecular Level. *Phys. Chem. Chem. Phys.* **2006**, *8*, 2539−2545.
(22) Pyykkö, P.; Patzschke, M.; Suurpere, J. Calculated Structures of $[Au = C=Au]^{2+}$ and Related Systems. *Chem. Phys. Lett.* **2003**, *381*, 45−52.
(23) Barysz, M.; Pyykkö, P. Strong Chemical Bonds to Gold. High Level Correlated Relativistic Results for Diatomic $AuBe^+$, AuC^+, $AuMg^+$, and $AuSi^+$. *Chem. Phys. Lett.* **1998**, *285*, 398−403.
(24) Havel, J.; Peña-Méndez, E. M.; Amato, F.; Panyala, N. R.; Buršíková, V. Laser Ablation Synthesis of New Gold Carbides. From Gold-Diamond Nano-Composite As a Precursor to Gold-Doped Diamonds. Time-of-Flight Mass Spectrometric Study. *Rapid Commun. Mass Spectrom.* **2014**, *28*, 297−304.
(25) Cohen, Y.; Kolodney, E. Kinetic Energy Distributions of C^+, C_2^+, Au^+, AuC^+ and AuC_2^+ Emitted from a Gold Surface Following Single Impact of KeV C_{60}^-: Carbide Ions Formation via a Recombination Mechanism. *Nucl. Instrum. Methods Phys. Res., Sect. B* **2011**, *269*, 985−989.
(26) Cohen, Y.; Bernshtein, V.; Armon, E.; Bekkerman, A.; Kolodney, E. Formation and Emission of Gold and Silver Carbide Cluster Ions in a Single C_{60}^- Surface Impact at KeV Energies: Experiment and Calculations. *J. Chem. Phys.* **2011**, *134*, 124701.
(27) Gibson, J. K. Laser Ablation and Gas-Phase Reactions of Small Gold Cluster Ions, $Au_n^+(1 \le n \le 7)$. *J. Vac. Sci. Technol., A* **1998**, *16*, 653−659.
(28) Ticknor, B. W.; Bandyopadhyay, B.; Duncan, M. A. Photodissociation of Noble Metal-Doped Carbon Clusters. *J. Phys. Chem. A* **2008**, *112*, 12355−12366.
(29) Liu, H.-T.; Xiong, X.-G.; Diem Dau, P.; Wang, Y.-L.; Huang, D.-L.; Li, J.; Wang, L.-S. Probing the Nature of Gold−Carbon Bonding in Gold−Alkynyl Complexes. *Nat. Commun.* **2013**, *4*, 2201.
(30) Visser, B. R.; Addicoat, M. A.; Gascooke, J. R.; Lawrance, W. D.; Metha, G. F. Spectroscopic Observation of Gold-Dicarbide: Photodetachment and Velocity Map Imaging of the AuC_2 Anion. *J. Chem. Phys.* **2013**, *138*, 174310.
(31) León, I.; Yang, Z.; Wang, L.-S. Probing the Electronic Structure and Au−C Chemical Bonding in AuC_2^- and AuC_2 Using High-Resolution Photoelectron Spectroscopy. *J. Chem. Phys.* **2014**, *140*, 084303.
(32) Osborn, D. L.; Vogelhuber, K. M.; Wren, S. W.; Miller, E. M.; Lu, Y.-J.; Case, A. S.; Sheps, L.; McMahon, R. J.; Stanton, J. F.; Harding, L. B.; et al. Electronic States of the Quasilinear Molecule Propargylene (HCCCH) from Negative Ion Photoelectron Spectroscopy. *J. Am. Chem. Soc.* **2014**, *136*, 10361−10372.
(33) Wu, X.-N.; Ma, J.-B.; Xu, B.; Zhao, Y.-X.; Ding, X.-L.; He, S.-G. Collision-Induced Dissociation and Density Functional Theory Studies of CO Adsorption over Zirconium Oxide Cluster Ions: Oxidative and Nonoxidative Adsorption. *J. Phys. Chem. A* **2011**, *115*, 5238−5246.
(34) Xu, B.; Meng, J.-H.; He, S.-G. Photoreaction Study of Methanol Adsorption Complexes on $VO_2(V_2O_5)_n^+$ (n = 1−3) Clusters at 355 nm. *J. Phys. Chem. C* **2014**, *118*, 18488−18495.
(35) Liu, Q.-Y.; Hu, L.; Li, Z.-Y.; Ning, C.-G.; Ma, J.-B.; Chen, H.; He, S.-G. Photoelectron Imaging Spectroscopy of MoC^- and NbN^- Diatomic Anions: A Comparative Study. *J. Chem. Phys.* **2015**, *142*, 164301.
(36) Xu, B.; Zhao, Y.-X.; Ding, X.-L.; Liu, Q.-Y.; He, S.-G. Collision-Induced Dissociation and Infrared Photodissociation Studies of Methane Adsorption on $V_5O_{12}^+$ and $V_5O_{13}^+$ Clusters. *J. Phys. Chem. A* **2013**, *117*, 2961−2970.
(37) Ho, J.; Ervin, K. M.; Lineberger, W. C. Photoelectron Spectroscopy of Metal Cluster Anions: Cu_n^-, Ag_n^-, and Au_n^-. *J. Chem. Phys.* **1990**, *93*, 6987−7002.
(38) Frisch, M. J.; Trucks, G. W.; Schlegel, H. B.; Scuseria, G. E.; Robb, M. A.; Cheeseman, J. R.; Scalmani, G.; Barone, V.; Mennucci, B.; Petersson, G. A.; et al. *Gaussian 09*; Gaussian Inc.: Wallingford, CT, 2009.
(39) Schäfer, A.; Huber, C.; Ahlrichs, R. Fully Optimized Contracted Gaussian Basis Sets of Triple Zeta Valence Quality for Atoms Li to Kr. *J. Chem. Phys.* **1994**, *100*, 5829−5835.
(40) Dolg, M.; Stoll, H.; Preuss, H. Energy-Adjusted *ab initio* Pseudopotentials for the Rare Earth Elements. *J. Chem. Phys.* **1989**, *90*, 1730−1734.
(41) Tao, J.; Perdew, J. P.; Staroverov, V. N.; Scuseria, G. E. Climbing the Density Functional Ladder: Nonempirical Meta−Generalized Gradient Approximation Designed for Molecules and Solids. *Phys. Rev. Lett.* **2003**, *91*, 146401.
(42) Wang, L.-N.; Zhou, Z.-X.; Li, X.-N.; Ma, T.-M.; He, S.-G. Thermal Conversion of Methane to Formaldehyde Promoted by Gold in $AuNbO_3^+$ Cluster Cations. *Chem. - Eur. J.* **2015**, *21*, 6957−6961.
(43) Meng, J.-H.; He, S.-G. Thermal Dihydrogen Activation by a Closed-Shell $AuCeO_2^+$ Cluster. *J. Phys. Chem. Lett.* **2014**, *5*, 3890−3894.
(44) Zeng, Q.; Chu, X.; Yang, M.; Wu, D.-Y. Spin−Orbit Coupling Effect on Au−C_{60} Interaction: A Density Functional Theory Study. *Chem. Phys.* **2012**, *395*, 82−86.
(45) Knowles, P. J.; Hampel, C.; Werner, H. J. Coupled Cluster Theory for High Spin, Open Shell Reference Wave Functions. *J. Chem. Phys.* **1993**, *99*, 5219−5227.
(46) Knowles, P. J.; Hampel, C.; Werner, H. J. Erratum: "Coupled Cluster Theory for High Spin, Open Shell Reference Wave Functions" [J. Chem. Phys. 99, 5219 (1993)]. *J. Chem. Phys.* **2000**, *112*, 3106−3107.
(47) Schlegel, H. B. Optimization of Equilibrium Geometries and Transition Structures. *J. Comput. Chem.* **1982**, *3*, 214−218.
(48) Gonzalez, C.; Schlegel, H. B. An Improved Algorithm for Reaction Path Following. *J. Chem. Phys.* **1989**, *90*, 2154−2161.
(49) Gonzalez, C.; Schlegel, H. B. Reaction Path Following in Mass-Weighted Internal Coordinates. *J. Phys. Chem.* **1990**, *94*, 5523−5527.
(50) Mozhayskiy, V. A.; Krylov, A. I. *ezSpectrum 3.0*. http://iopenshell.usc.edu/downloads (accessed May 29, 2015).
(51) Seburg, R. A.; Patterson, E. V.; McMahon, R. J. Structure of Triplet Propynylidene (HCCCH) as Probed by IR, UV/vis, and EPR Spectroscopy of Isotopomers. *J. Am. Chem. Soc.* **2009**, *131*, 9442−9455.
(52) Stanton, J. F.; Garand, E.; Kim, J.; Yacovitch, T. I.; Hock, C.; Case, A. S.; Miller, E. M.; Lu, Y.-J.; Vogelhuber, K. M.; Wren, S. W.; et al. Ground and Low-Lying Excited States of Propadienylidene (H_2C═C═C:) Obtained by Negative Ion Photoelectron Spectroscopy. *J. Chem. Phys.* **2012**, *136*, 134312.
(53) Seburg, R. A.; McMahon, R. J. Automerizations and Isomerizations in Propynylidene (HCCCH), Propadienylidene (H_2CCC), and Cyclopropenylidene (c-C_3H_2). *Angew. Chem., Int. Ed. Engl.* **1995**, *34*, 2009−2012.
(54) Seburg, R. A.; Patterson, E. V.; Stanton, J. F.; McMahon, R. J. Structures, Automerizations, and Isomerizations of C_3H_2 Isomers. *J. Am. Chem. Soc.* **1997**, *119*, 5847−5856.

DOI: 10.1021/acs.jpca.5b05122
J. Phys. Chem. A XXXX, XXX, XXX−XXX